Regional Studies in Marine Science 31 (2019) 100740

Contents lists available at ScienceDirect

Regional Studies in Marine Science

journal homepage: www.elsevier.com/locate/rsma

Physical dynamics of the reef flat, channel, and fore reef areas of a fringing reef embayment: An oceanographic study of Pago Bay, Guam

Christina M. Comfort [a,*], Gordon O. Walker [a], Margaret A. McManus [a], Atsushi G. Fujimura [b], Chris E. Ostrander [c], Terry J. Donaldson [b]

[a] Department of Oceanography, University of Hawaii at Manoa, Honolulu, HI 96822, USA
[b] Marine Laboratory, University of Guam, Mangilao, GU 96923, USA
[c] University of Utah, Salt Lake City, UT 84112, USA

HIGHLIGHTS

- Circulation in the Pago Bay reef flat and channel is strongly driven by wave height.
- Circulation on the fore reef is affected by wave height and wind.
- The reef flat experienced diel temperature shifts with a range as large as 12.8 °C.
- Pulses of relatively cooler water were observed at 16-26 m depth.
- Heavy rain events can cause dramatic changes in channel water quality.

ARTICLE INFO

Article history:
Received 8 January 2019
Received in revised form 7 May 2019
Accepted 21 June 2019
Available online 5 July 2019

Keywords:
Shelf dynamics
Coastal oceanography
Nearshore currents
Water quality
Water temperature
USA
Territory of Guam
Pago Bay

ABSTRACT

Long-term observations of oceanographic patterns and processes provide necessary context for integrative ecological studies and for assessing and mitigating anthropogenic impacts to coastal ecosystems. The oceanographic patterns and processes of Pago Bay, Guam, a tropical coral reef system with a small estuary, were observed for one year. An array of 50 sensors including current profilers, temperature and dissolved oxygen loggers, and water quality sensors were deployed throughout Pago Bay from 0–26 m depth. Water flow was primarily driven by wave height in the reef flat and channel. In addition, wind and wave directions that were directly across-shore contributed to faster flow speeds throughout the bay. On the fore reef, wave height was the strongest predictor of current speed, but wind direction had a strong influence on current direction. Flow in the channel and on the reef flat was more tightly tied to environmental factors of wind and waves than flow on the fore reef. Extreme daily temperature variations on the reef flat were observed. In deeper water, cold pulses were observed, indicating that large internal waves may propagate around the slopes of Guam. Cold pulses may deliver nutrients to shallower ecosystems and periodically cool deeper areas of the fore reef. In response to heavy rain events, the estimated backscatter in the channel increased sharply along with significant changes in other water quality parameters. Rain events of this magnitude and associated backscatter increases occur frequently. Along with soil-destabilizing land use practices in the Pago River watershed, the current flow and water quality observations presented here indicate that sedimentation may be a risk for the Pago Bay fore reef coral habitat. The understanding of circulation, thermal environment, and rainstorm impacts in this fringing reef system provides a baseline for understanding the ecology, coral reef resilience, and future oceanographic changes in Pago Bay.

1. Introduction

Understanding physical oceanographic processes and patterns is essential to a comprehensive understanding of any marine ecosystem. Some ecologically relevant physical parameters include flow dynamics, temperature, variability in oceanographic parameters such as pH and nutrients, and in nearshore systems, land-based freshwater and sediment inputs. These physical and geochemical forcing mechanisms contribute to the distribution of species (Fulton et al., 2005; McClanahan and Maina, 2003), productivity of the ecosystem (Hatcher, 1990), and vulnerability of the ecosystem to climate change and other anthropogenic stressors (Fabricius, 2005; Nyström et al., 2000; Pastorok and

* Correspondence to: Department of Oceanography, University of Hawaii at Manoa, 1000 Pope Road, Honolulu, HI 96822, USA.
E-mail address: ccomfort@hawaii.edu (C.M. Comfort).

https://doi.org/10.1016/j.rsma.2019.100740

Bilyard, 1985). In this study, we investigate the oceanographic patterns and processes of a large fringing reef embayment, Pago Bay, which is located on the east side of the island of Guam in the Mariana Islands (Fig. 1).

Circulation in fringing reef environments and estuarine embayments

Complex coastlines with fringing coral reefs typically have flow that is driven by waves, tides, and wind (e.g., Storlazzi et al., 2004; Taebi et al., 2011). In fringing reef environments, waves breaking over the reef crest move water onto the reef flat, leading to wave driven pressure gradient setups that eventually drive flow towards excurrent channels (Marsh et al., 1982; Vetter et al., 2010; Lowe et al., 2009; Clark, 2013). Wind driven flows are another mechanism driving flow in fringing reef systems (Storlazzi et al., 2006, 2004) and coastal embayments (Ostrander et al., 2008). On the deeper fore reef areas, tidal forcing often has a more dominant influence on flow (Storlazzi et al., 2004; Vetter et al., 2010). Buoyancy flows can also be important and can be caused by onshore–offshore salinity and/or temperature gradients and vertical stratification (Monismith et al., 2006).

Previous research on circulation on the reef flat of Pago Bay, Guam found that most areas of the reef flat follow the typical pattern of flow draining towards the channel, but restricted circulation cells with longer water retention times were observed in two areas of Pago Bay (Marsh et al., 1982). Using current profilers deployed over a full year, this study is the first long term observation of current flow on the Pago Bay reef flat, and additionally includes yearlong observations of current flow in the Pago Bay channel and on the fore reef. We were also able to calculate current ellipses and assess how environmental factors such as wind, waves, and tides affect flow throughout the bay. These long-term observations allow for improvement and expansion on the existing conceptual model of Pago Bay's circulation (Marsh et al., 1982).

Diel and seasonal patterns in fringing reef environments

Diel to seasonal fluctuations in multiple oceanographic parameters, including current velocity, temperature, dissolved oxygen, and pH, among others, were assessed in this study. Due to the transitional nature of fringing reef environments (land – shallow reef flat – open ocean), high variability in the physical environment may be observed. On daily scales, trade winds (the prevailing wind pattern in tropical latitudes, from the northeast to east in the northern hemisphere) tend to increase during the day and slacken at night, and these diel changes in wind forcing coupled with land based terrigenous input can cause diel increases in turbidity (Piniak and Storlazzi, 2008). Shallow back reef areas can experience extreme diel variations in water temperature, which affects organism ecophysiology (Craig et al., 2001; Putnam and Edmunds, 2011). In shallow coastal areas, tides can have a large impact on flow and waves (Becker et al., 2014) and other physical factors such as light availability (Anthony et al., 2004). On seasonal scales, riverine and groundwater input to fringing reef systems can vary, altering the salinity and nutrient input to the very nearshore environment, and turbid river flows are likely to be more common in rainy season. Understanding the natural variability of a system is essential to assessing the systems' vulnerability to anthropogenic impacts and may provide important insight into the overall community structure and function.

Overall, this study provides a description of the oceanographic patterns and processes of Pago Bay, Guam. These new insights into Pago Bay provide a strong contextual baseline for future marine ecological and biological studies in the region. The long time series of observations obtained in the study provided an opportunity to assess the impact of a major rain event in the context of a year of continuous observational data.

2. Methods

2.1. Study site

Pago Bay is a 1.5 km^2 embayment on the eastern side of the island of Guam (Fig. 1). The primary freshwater input into the bay is from Pago River. Two inland rivers, Lonfit River and Sigua River, feed into Pago River, which enters in the southern part of Pago Bay and discharges to the Pacific Ocean via the Pago Channel (Fig. 1). The bay is a popular fishing area in the local community and in recent years large sediment inputs to the bay due to erosion from coastal and inland development have been observed, with unquantified effects on the bay's ecosystem. The average rainfall in the Pago watershed is 288.29 cm per year (USGS Mt. ChaChao rain gauge; 2006–2015 approved data). The region experiences a wet season (July–November) and dry season (December–June) (http://ns.gov.gu/climate.html). Easterly to northeasterly trade winds are dominant (https://w2.weather.gov/climate/index.php?wfo=guam). Typhoon season in the western Pacific is generally between May–October, although no typhoons occurred during our study period. Tides in Guam are mixed semidiurnal. The mean tidal range is about 0.5 m, with neap and spring tidal ranges from 0.3–0.8 m.

Pago Bay was divided into four distinct habitat zones that were examined in this study: the Pago River channel, the shallow reef flats flanking the channel, an abrupt reef crest where wave energy is dissipated, and a fore reef (Fig. 2). The channel is about 140 m wide and reaches depths of up to ∼30 m near its entry to the Pacific Ocean. The reef flat and reef crest areas are shallow, with some areas exposed during low tide. At its widest area near the channel, the reef flat extends about 715 m from shoreline to reef crest, and the narrower area in the northern part of the bay is about 185 m wide. The benthos of the channel is generally uncolonized and a mix of sand and mud; the benthic community of the reef flat and reef crest is made up of turf algae, crustose coralline algae, and macroalgae, with some inshore areas of seagrass; the fore reef is a complex coral reef habitat with 10%–50% coral cover, and has a slope of about 4.7–8.9 degrees between 0–20 m depth (NOAA National Center for Coastal Ocean Science, https://products.coastalscience.noaa.gov/collections/benthic/default.aspx, accessed 17 September 2018; Google Earth).

2.2. Instrumentation and study objectives

Fifty instruments were deployed in the channel, reef flat, reef crest, and fore reef during the planned study period of 8 August 2016–24 July 2017 (Fig. 3). An additional current profiler was deployed from 9 March 2018–7 May 2018 to gather data about the southern part of the reef flat (Fig. 2). Our overall goal was to observe temporal and spatial patterns of current flow and water properties in the bay to better understand the physical dynamics of the bay and provide baseline information for future ecological studies.

2.3. Calibration and programming

The compass of each current profiler was calibrated according to instructions in the user manuals (SonTek/YSI, 2000; Nortek, 2017). The HOBO® Dissolved Oxygen Logger (U26-001) was calibrated using the "100% saturation method" both before and after each deployment to address drift that may have occurred during the deployment (Onset, 2012). The reference spectrum of the Satlantic SUNA V2 was updated prior to each deployment using deionized water (Satlantic, Inc., 2016). The Sea Bird Electronics 16plus V2 SeaCAT CTP Recorder, Sea Bird Electronics 63 Optical

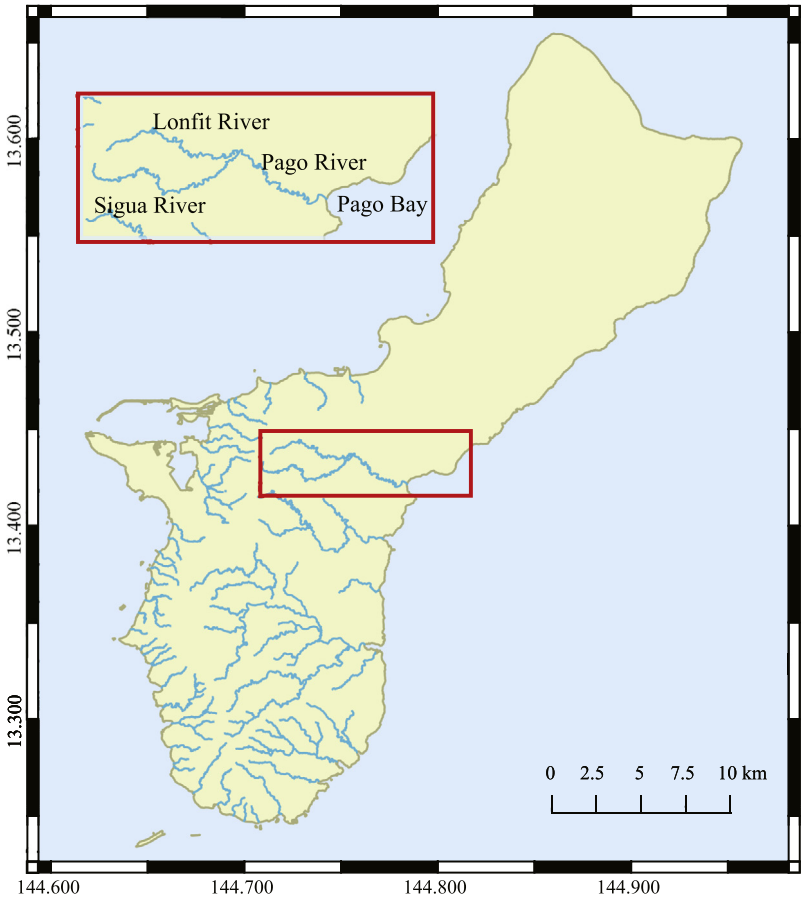

Fig. 1. Map of Guam showing major rivers. The inset in orange highlights the rivers that drain the Pago watershed and the study site, Pago Bay. GIS data: University of Guam Water and Environmental Research Institute of the Western Pacific.

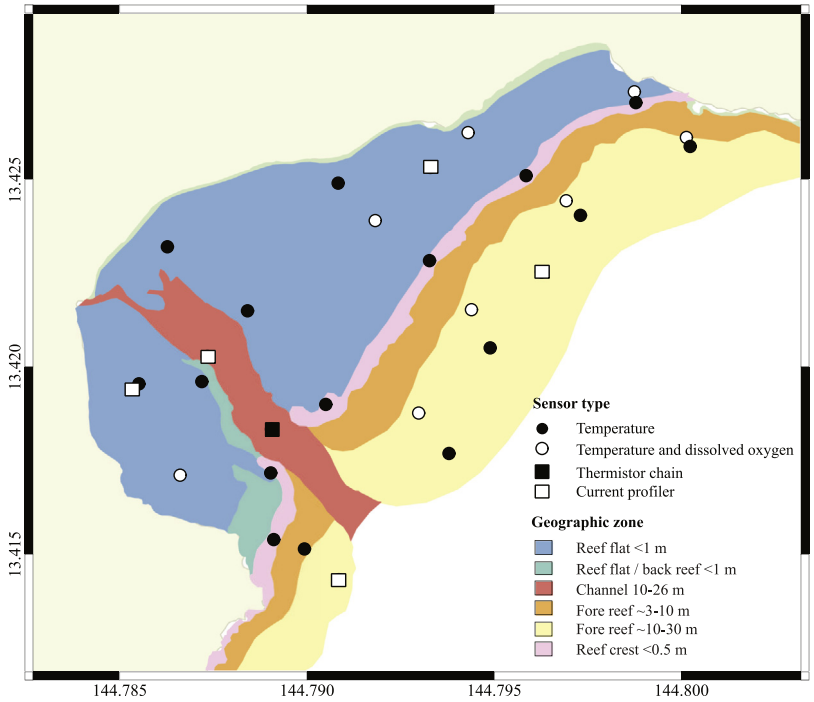

Fig. 2. Map of Pago Bay with locations of sensors plotted over geographic zones as they are referred to in this study. Geographic zone data from NOAA's National Centers for Coastal Ocean Science (NCCOS) (https://products.coastalscience.noaa.gov/collections/benthic/e99us_pac/default.aspx, accessed 17 September 2018).

Table 1
Instrumentation details including instrument type, parameters the instrument measured, in what zones (channel, fore reef, reef flat, reef crest) the instruments were deployed, the sampling intervals used, and the depths of deployment.

Instrument	Parameters measured	Location (# instruments)	Sampling rate	Depth deployed
Sontek acoustic Doppler profiler 1000 kHz	Current magnitude and direction, estimated backscatter, pressure	Channel (1); Fore reef (2)	10, 20, or 30 min	10 m (channel)[a]; 15 m (fore reef)
Nortek acoustic Doppler current profiler 2000 kHz	Current magnitude and direction, pressure	Reef flat (2)	10 min	1 m
HOBO TidBit[b]	Temperature	Reef flat (5); Reef crest (6); Fore reef (5)	5 or 10 min	<1 m (reef flat, reef crest); 15 m (fore reef)
HOBO Dissolved Oxygen Logger (U26-001)	Dissolved oxygen, temperature	Reef flat (4); Fore reef (6)	10 min	<1 m (reef flat); 7 m (fore reef)
HOBO TidBit	Temperature	Channel (2)	1 or 5 min	25.4 m; 5.7 m
HOBO Water Level Logger (vertical temperature chain)	Pressure, temperature	Channel (12)	1 min	25 m to 6 m
Sea Bird Electronics 16plus V2 SeaCAT CTP Recorder	Temperature, conductivity, pressure	Channel (1)	30 min	10 m[a]
WETlabs ECO FLNTU (integrated with SeaCAT)	Fluorescence, turbidity	Channel (1)	30 min	10 m[a]
Sea Bird Electronics 63 (integrated with SeaCAT)[c]	Dissolved oxygen	Channel (1)	30 min	10 m[a]
Satlantic SUNA V2	Nitrate	Channel (1)	5 min	10 m[a]
Satlantic SeaFET	pH, temperature	Channel (1)	1 min	10 m[a]

[a]On deployment 1, these instruments were deployed at 13 m.
[b]On some deployments, HOBO Pendants were used to measure temperature instead of TidBits.
[c]On deployment 2, a HOBO Dissolved Oxygen logger sampling at 10 min interval replaced this sensor.

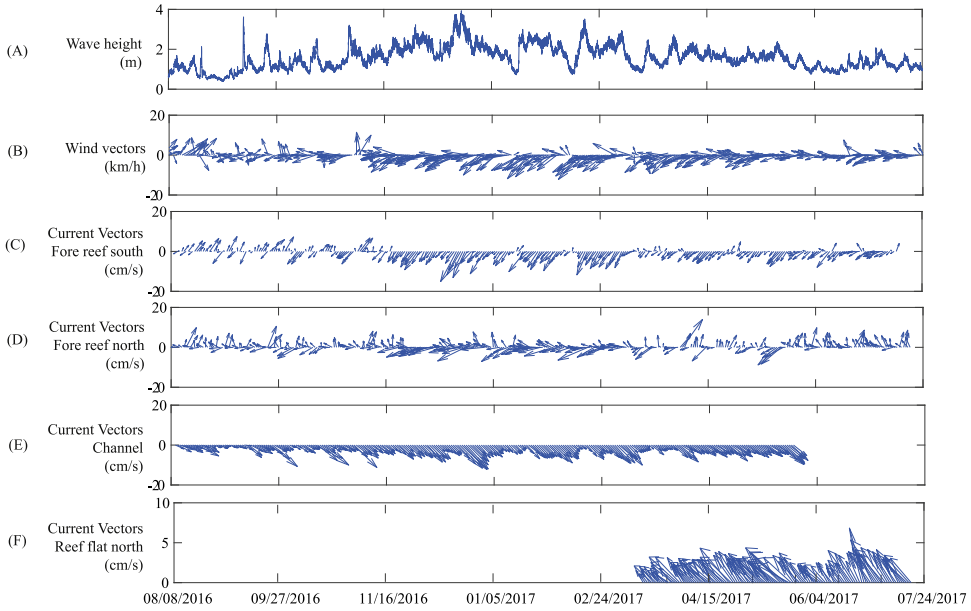

Fig. 3. Time series observations from August 2016–July 2017 of (A) wave height, (B) wind magnitude and direction, (C) subtidal currents on the south fore reef, (D) subtidal current vectors on the north fore reef, (E) subtidal current vectors in the channel, and (F) subtidal current vectors on the north reef flat. Date format on the *x*-axis is MM/DD/YYYY.

Dissolved Oxygen, WET Labs ECO FLNTU, the Satlantic SeaFET, and HOBO Tidbit sensors were factory calibrated.

Instruments' sampling rates ranged from 1 min to 30 min depending on battery life and deployment length (Table 1). Planned deployment lengths ranged from 2 to 7 months, which resulted in some differences in programming strategy throughout the study. Sampling rate details by deployment are shown in Table S1.

2.4. Deployments

Instruments were deployed using snorkel, SCUBA, and over-the-side boat deployment techniques, depending on the depth, size, and location of sensors and moorings. A short summary of the field deployments follows; technical details of each deployment can be found in the Supplement.

Current profilers were deployed in the channel, the reef flat north and south of the channel, and the fore reef north and south

of the channel (Fig. 3, Table 1). The current profilers were moored on the seafloor and upward-looking (Fig. S1). Temperature loggers and dissolved oxygen loggers were attached to the substrate throughout the bay in areas of sand, rubble, or rock (avoiding live coral) (Figs. S2, S3). The thermistor chain was anchored to silty substrate and suspended with a subsurface mooring ball at 5 m depth to avoid entanglements with boat traffic in the channel. Temperature chain data were collected in a series of discrete deployments: a 2-month deployment from August–October 2016, and a series of 1-month deployments during November 2016, March 2017, June 2017, and July 2017. Pressure sensors were deployed at the top and bottom of the water column from March 2017 onward to determine the effect of current on the angle of the thermistor chain, and these data were used to calculate actual sensor depths. A CTD with integrated dissolved oxygen, fluorescence, and turbidity sensors, a pH sensor, and a nitrate sensor (Table 1) was deployed alongside the current profiler in the Pago Bay channel (Fig. S4).

2.5. Data recovery

Data were recovered successfully from most instruments throughout the year-long deployment (Table S2). Current magnitude and direction data were obtained from the all current profilers except the May–July 2017 deployment in the channel due to a malfunctioning beam. There were other issues that caused minor data loss: Biofouling issues caused oxygen sensors to record unrealistic dissolved oxygen data from August 2016–March 2017; a suite of instruments needed repair during deployment 2 (October 2016–March 2017); and problems with the nitrate sensor calibration and drift in the deployments 3 and 4 resulted in unreliable data.

2.6. Data analyses

2.6.1. Spatial and temporal current patterns in Pago Bay

Current data were separated into categories based on wind and wave conditions. Trade wind conditions were defined as mean daily wind directions between 30–120°. Any other mean daily wind direction was defined as non-trade wind conditions. Large waves were defined as a daily mean greater than 1.5 m, which was the median observed significant wave height throughout the time series. Small waves were defined as a daily mean significant wave height less than 1.5 m. The resulting four categories were: trade winds/large waves, trade winds/small waves, non-trade winds/large waves, and no-trade winds/small waves.

Current magnitude and direction at subtidal frequencies were evaluated by filtering the data using a low-pass Butterworth filter with a cutoff of 33 h (Ryan et al., 2008). Mean subtidal current vectors during each environmental category were calculated. Near-surface and near-bottom current ellipses (representing perturbations from the mean) were calculated for each current profiler location and each wind and wave category. Generalized additive modeling (GAM) was employed to determine any statistical significance of environmental forcing and its effects on current velocity.

2.6.2. Generalized additive modeling (GAM) of environmental drivers of current speed

GAMs are similar to general linear models (GLM) but allow relationships between predictors and the response variable to be nonlinear. GAMs were fit to investigate the importance of various environmental drivers of current velocity in Pago Bay at each of the current profiler locations. The predictor variables assessed were wave direction, wave height, wind speed, wind direction, and daily cumulative tidal change. Pearson correlation coefficients and analysis of variance inflation factors (VIFs, for multicollinearity) indicated that wind speed and wave height were correlated, and wind direction and wave direction were correlated (VIF $>$ 3) (Zuur et al., 2010; Zuur, 2012). Therefore, multiple model runs were constructed to avoid collinearity bias while still investigating all parameters. Wind direction was smoothed using a cubic spline to set 360 degrees equal to zero degrees. All other covariates were smoothed using a thin plate regression spline (including wave direction, which only varied in a narrow window). A smoothed variable, day, was included in every model run to help account for temporal autocorrelation.

The GAMs were constructed for each location type (reef flat, channel, and fore reef) using the gamma distribution and a log link function. No GAM was constructed for the reef crest because current velocity measurements were not taken in this location. The response variable distributions better approximated normal distributions when separated by location type. The channel, north reef flat, and south reef flat locations were modeled individually; for the fore reef, the north and south locations were modeled together using a random factor to account for the two separate deployments in this location type. All possible model combinations were assessed using the R package "dredge". The presented model for each location type was selected by the lowest Akaike information criteria with a correction for small sample sizes (AICc) where the model included only statistically significant smoothers.

Statistical modeling for water speed was carried out in R (R Core Team, 2017) using the mcgv, car, AICcmodavg, MuMIn, and lattice packages (Barton, 2009; Fox et al., 2012; Mazerolle and Mazerolle, 2017; Wood, 2001; Sarkar, 2008).

2.6.3. Temperature and oxygen mapping in Pago Bay

Data from temperature and oxygen sensors deployed throughout the bay were analyzed for spatial and temporal trends. Spectral analysis was used to identify the dominant scales of variability. An animated map of temperature measurements (August 2016–July 2017) was created using gridded interpolation between daily means to illustrate seasonal variability and spatial variation throughout the bay. Additionally, we investigated two hypotheses regarding dissolved oxygen concentrations: (1) higher wind speed can cause higher gas exchange rates, so higher wind will be correlated with a higher dissolved oxygen concentration; (2) higher current speeds will correlate with higher dissolved oxygen measurements. All calculations were done in MatLab (Mathworks, 2017).

2.6.4. Water column temperature and cold pulses

Temperature time-series records from the temperature chain were investigated using spectral analysis to determine dominant scales of variability throughout the water column and between seasons. Pulses of relatively cooler near-bottom water in Pago Bay were identified in the lower water column. Cold pulses are intrusions of colder water into a shallower environment, often driven by internal waves (McManus et al., 2008). In this study, cold pulses were defined as a decrease in temperature of at least 0.3 °C in a span of 5 min. In Hawaii, pulses with 0.5 °C lower temperature were associated with significant changes in backscatter and phytoplankton measurements (Sevadjian et al., 2012), and based on visual inspection of the time series data, this cutoff captured the anomalous decreases in temperature, but avoided the more typical fluctuations which occurred more slowly. Cold pulse identification was carried out for all temperature records throughout the water column to determine how far up the water column the cold pulse was detectable. If cold pulses were identified in the mid to upper water column but were not connected to a bottom-up pulse, they were likely not related to internal waves and therefore not included in this analysis. The length of each cold pulse was defined as the time it took for the temperature to recover by 50% (after Sevadjian et al., 2012).

2.6.5. Pago Bay channel: Oceanographic parameters and response to an extreme storm event

For all measured parameters, spectral analysis was used to determine important timescales of variability under normal conditions. Then, the measured oceanographic parameters – temperature, salinity, oxygen, fluorescence, turbidity, nitrate, and pH – were investigated for a response to a heavy storm event on April 23–28, 2017. Statistics for each parameter were compared for the period 14 days prior to the storm event (baseline conditions) and the period of 5 days during storm event. The most extreme observations during the storm event were compared to the baseline levels.

Estimated backscatter was calculated from the measured echo intensity at the channel and fore reef current meters deployment following the methods of Deines (1999). A GAM was constructed to investigate the effects of rain and wave height on estimated backscatter. A smoothed variable for "day" was included to help account for temporal autocorrelation. The model was constructed using the gamma distribution and a log link function.

2.7. Environmental data

Rain data from the USGS rain gauge at Mt. Chachao and from the University of Guam campus were used in the study. Data from the USGS rain gauge were downloaded from (https://waterdata.usgs.gov/gu/nwis/inventory/?site_no=132617144423366&agency_cd=USGS), and data from the University of Guam rain gauge were provided by Mark Lander (WERI, University of Guam, pers. comm.).

Wind data were downloaded from the NOAA National Weather Service data archives for the Guam International Airport (https://w2.weather.gov/climate/index.php?wfo=guam).

Wave data (wave height and direction) were collected by a PacIOOS wave buoy deployed in Ipan, Guam and downloaded from http://www.pacioos.hawaii.edu/waves/buoy-ipan/. The buoy is located about 7 km south of Pago Bay.

3. Results

3.1. Spatial and temporal current patterns in Pago Bay

Time series records of wind, waves, and currents in Pago Bay showed that the flow on the fore reef changed direction depending on environmental conditions, while the flow on the reef flat and channel was more consistent in direction. The current magnitude was positively correlated with wave height at all sites (Figs. 3, 4).

Of the days of our study with current data, 53.6% had trade winds with large waves, 29.8% had trade winds with small waves, 1.3% had non-trade winds and large waves, and 15.3% had non-trade winds and small waves. The average subtidal flow on the reef flat was fastest during large wave and trade wind conditions (north reef flat: 17.9 cm/s, south reef flat: 8.7 cm/s), and slower during trade winds and small wave conditions (north reef flat: 13.1 cm/s, south reef flat: 2.6 cm/s) (Fig. 5). Trade winds drove the flow inshore on the southern reef flat (Fig. 5B). In the channel, the currents consistently flowed out towards the open ocean regardless of environmental forcing. The mean flow speed in the channel was 13.8 cm/s with trade winds and large waves, and 8.9 cm/s with trade winds and small waves. Similar patterns were observed for non-trade conditions.

On the fore reef, the observed magnitudes were slower than in other regions, but the fastest current speeds also occurred during large waves and trade wind conditions (3.5 cm/s on the southern fore reef and 1.8 cm/s on the northern fore reef). The south fore reef flow tended to reverse direction depending on the wind, with trade winds leading to alongshore flow in the southwest direction, and non-trade winds leading to alongshore flow in the northeast direction.

Current ellipses (showing perturbations around the mean velocity) showed largely consistent patterns during different environmental conditions (Fig. S5). Variation in flow was typically alongshore on the fore reef. The primary axis of variation was in the same direction as the mean flow on the reef flat and channel. Shear between the upper and lower water column was observed in the channel during all conditions except non-trade winds with small waves (Fig. S5D).

3.2. Environmental drivers of current speed

Current speed (*waterspeed*) in Pago Bay was found to correlate to wave height (*waveheight*) and direction (*wavedir*), wind direction (*winddir*), and spring/neap tidal cycles (*tidechange*) using the best-fit GAMs. The best-fit models for water speed at each location were chosen by finding the combination of significant smoothers with the lowest AICc score. The two fore reef locations responded similarly to environmental shifts and were modeled together, using the factor of "site" to account for differences in the shape of the response between the two sites. A smoother for "day" was included to help reduce residual structure from temporal autocorrelation. The following models were selected:

Channel:

$$waterspeed \sim s(waveheight) + s(tidechange) + s(wavedir) + s(day)$$

Fore reef:

$$waterspeed \sim s(waveheight, by = site) + s(winddir, bs = \text{“}cc\text{”}) + s(day, by = site) + s(tidechange) + site$$

Reef flat (north):

$$waterspeed \sim s(waveheight) + s(day) + s(tidechange) + s(wavedir) + s(winddir, bs = \text{“}cc\text{”})$$

Reef flat (south):

$$waterspeed \sim s(waveheight) + s(day) + s(winddir, bs = \text{“}cc\text{”})$$

Results of the selected GAMs are shown in Table 2. Statistics, estimates, and significance for each model variable are shown in Table S3. Residual plots and other goodness of fit assessments are shown in the supplement (Figs. S6–S9).

In the channel, the GAM showed primarily wave-driven flow (Fig. 6). A model with only wave height and a smoother for temporal autocorrelation explained 65% of the variation in current speed. Adding wave direction resulted in an increase in percent deviance explained to 72.6%. The smoothers for wave height and wave direction were significant. Flow speed increased with increasing wave height, and wave directions approaching directly across shore were also associated with faster flow speeds. Days with spring tides had slightly faster flow than days with neap tides. The relationship was significant and increased the percent deviance explained to 74.5%.

On the northern reef flat, the model investigation resulted in a best-fit model showing significant positive relationships for wave height and a negative relationship with the daily mean tide fluctuation. A model with only wave height and a smoother for temporal autocorrelation factor explained 72.4% of the variation. Wave directions that were closer to directly across shore increased the water speed on the reef flat (Fig. 6). The smoother for wave direction increased the deviance explained to 83%. The smoother for wind direction showed an increase in water speed as wind turned more across-shore, and increased the deviance

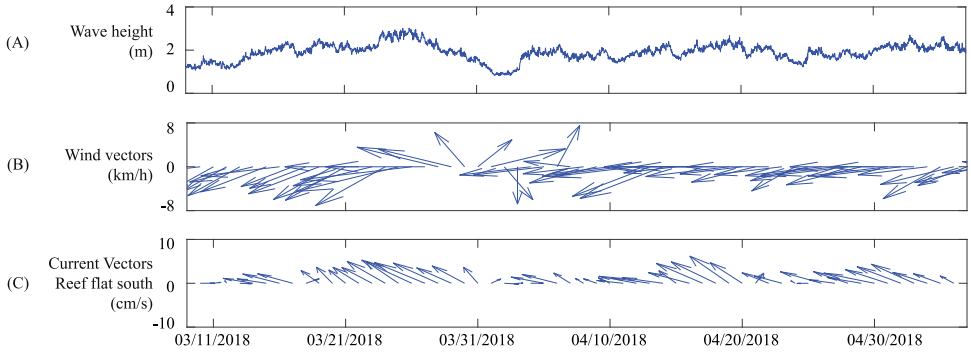

Fig. 4. Time series observations from March 2018–May 2018 of (A) wave height, (B) wind magnitude and direction, (C) subtidal currents on the south reef flat. Date format on the *x*-axis is MM/DD/YYYY.

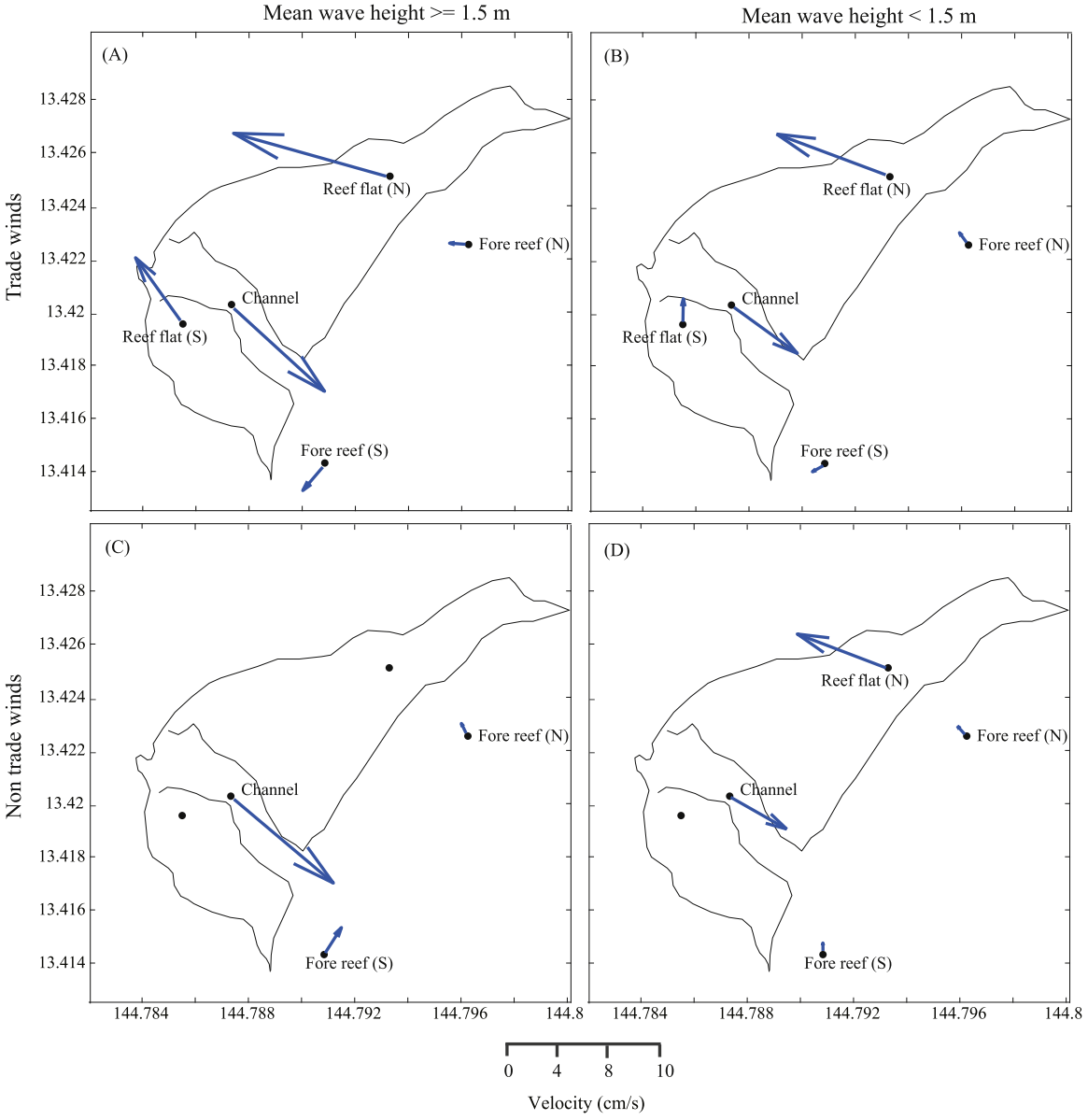

Fig. 5. Subtidal flow magnitude and direction at each current profiler location under four types of environmental conditions. (A) Trade winds and large waves, (B) trade winds and small waves, (C) non-trade winds and large waves, and (D) non-trade winds and small waves. Where arrows are missing, there were no available data during that environmental condition category.

Table 2
R-squared values and % deviance explained for each of the selected models.

Location	Smoother	p-value	Adjusted R^2	% Deviance explained
Channel	Wave height Spring–neap tide Wave direction	<0.001 <0.001 <0.001	0.71	74.5
Fore reef	Wave height (south) Wave height (north) Wind direction Spring–neap tide	<0.001 <0.001 <0.001 0.006	0.528	55.1
Reef flat north	Wave height Spring–neap tide Wave direction Wind direction	<0.001 <0.001 <0.001 <0.001	0.869	88.8
Reef flat south	Wave height Wind direction	<0.001 0.04	0.937	94.8

explained to 87.6%. The large confidence intervals in the westerly directions reflect that there were few days with observations of west winds, so that part of the smoother should be interpreted with caution. During extreme low tides, much of the reef flat was dry and exposed, and relatively little water was pushed over the reef crest by waves. The effect on the model was small, increasing deviance explained to 88.8%, but the smoother was significant and decreased AICc score by 12.

The southern reef flat had the best-fitting model with 94.8% of deviance explained. Most of the deviance in current speed was explained by wave height alone, and wind direction had a significant but smaller effect in which across-shore wind correlated to faster flow speeds (Fig. 6).

On the fore reef, the GAM verified that larger waves were associated with faster flow (Fig. 6). At larger wave heights, the flow was more strongly impacted at the southern fore reef than the northern fore reef. A model constructed with only wave height and a smoother for temporal autocorrelation explained 50.6% of the variation. When wind was across-shore in the same direction as the mean flow of the northern fore reef, water speed was faster, and additionally westerly wind was associated with higher flow rates (Fig. 6). Adding wind direction to the model increased the deviance explained to 54.5% and was significant. The spring/neap tidal cycle had a small positive correlation with flow speed, increasing the deviance explained to 55.1% with a significant smoother.

3.3. Temperature and oxygen mapping in Pago Bay

Benthic temperature data on the reef flat, fore reef, and channel were collected throughout the year of deployment (Media 1 — Supplement). Pago Bay experienced a very stable mean temperature throughout the year, with the difference in mean temperature between wet and dry season ranging only 0.18–1.55 °C at each sensor (Fig. 7). Differences in temperature between the reef flat and fore reef were similarly small. However, daily temperature variability was much higher on the reef flat (median 1.94 °C) than in deeper water on the fore reef (median 0.38 °C) (Fig. 7). Spectral analysis showed variability was primarily diel, indicating that daily solar insolation was the most influential factor controlling temperature both on the shallow reef flat and on the fore reef. The greatest temperature variation occurred on the southern reef flat in both wet and dry season with temperature variability as great as 12.38 °C in a single day, and spectral analysis showed that this variation occurred on a diel frequency.

Dissolved oxygen concentrations varied on diel time scales on the reef flat and on the fore reef. Oxygen was higher during the day by an average of 2.40 mg/l on the reef flat and 0.60 mg/l on the fore reef (tailed two sample t-test, $p < 0.001$). Spectral analysis revealed consistent variation at the 24 h period and harmonics. Reef flat daytime dissolved oxygen was positively correlated with temperature in the southern reef flat, and the strength of the correlation decreased moving northward (R^2 values, south to north on the reef flat: 0.78, 0.41, 0.17, 0.02). Regression analysis revealed no consistent trends between dissolved oxygen and wind speed in any location, or between dissolved oxygen and current speed.

3.4. Water column temperature in Pago Channel

The thermistor chain deployed in the channel measured water column temperature for a total of 203 recording days. Seasonal warming and cooling of the entire water column was observed (Fig. S10), along with diel heating that was observed through the entire water column (Fig. 8). Currents changed the angle of the thermistor chain throughout the deployment. The thermistor chain was moored at approximately 28 m, and the water profile depth coverage ranged from 6.0 m–24.0 m during low current speeds to 12.0 m–25.6 m during the fastest current speeds (Fig. 8).

Water temperature in Pago Bay fluctuates at semidiurnal M_2 (range 11.88–12.15 h) and diurnal (range 23.36–24.14 h) periods. Throughout the year, the top part of the water column warmed and cooled based on solar heating (Fig. 9). Near the benthos, diel heating was only observed during dry season (December–June).

A total of 109 cold pulses were identified during the time series (0.3 °C decrease in 5 min). Ninety of these cold pulses recovered within 3 h, 80 recovered within 2 h, and 30 recovered within 1 h. Comparisons of cold pulse occurrence frequency with oceanographic conditions showed that cold pulses were observed more often when sea surface temperature was higher than the mean yearly SST (Student's two-sample t-test, $p = 0.0038$) (Fig. 10). Cold pulses were detectable from the bottom of the water column (deepest sensor at ∼25 m depth) up to about 15 m depth, and they were observed more regularly during the wet season (July to November). Cold pulses were not observed in other fore reef temperature records, which were located at 14 and 7.6 m depth. This suggests that cold pulses propagate to ∼15 m depth but generally not shallower.

3.5. Oceanographic parameters in Pago Channel: Scales of variability and response to an extreme storm event

3.5.1. Oceanographic parameters in Pago Bay Channel

Oceanographic parameters, which included temperature, pH, dissolved oxygen, fluorescence and turbidity, were measured in the channel of Pago Bay in addition to currents (Fig. 11). Typical seasonality was observed in temperature, with warmer temperatures in the wet season (summer to fall) and cooler temperatures in the dry season (winter to spring). pH and oxygen did not

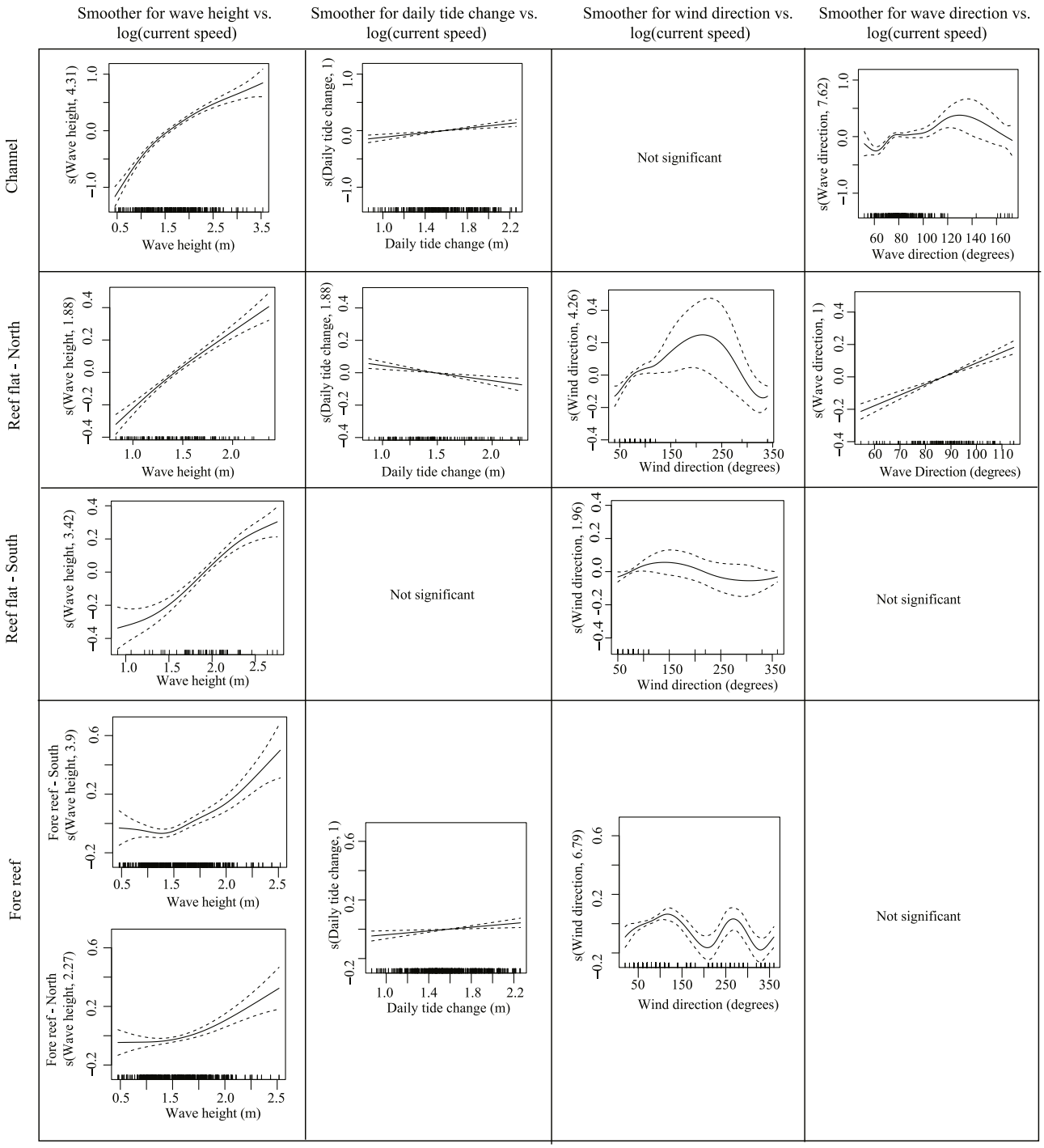

Fig. 6. Plots of the estimated smoothers for the selected GAM for water speed at each location. On all plots, the *x*-axis shows the covariate/forcing variable, and the *y*-axis shows the response of water speed. The response variable is scaled by the log relationship and centered around zero. The *y*-axis shows the centered smoothing function of the response variable for each covariate. The smoothing spline fits are the solid curves, and 95% confidence bands are shown as dashed lines.

show any seasonal trends. Increases in backscatter were more frequent during the rainy season. The shift to slightly higher values in oxygen during the March–July period co-occurred with the change of instrument, so cannot be attributed to seasonal trends.

Spectral analysis indicated that oxygen and fluorescence primarily varied at 24 h periodicity. Turbidity did not have consistent periodicity, with one deployment showing no significant spectral peaks, one showing a weak peak at 12 h, and another showing weak spectral peaks at 12.4 and 23.9 h. Variability in pH corresponded to both tidal periodicities (12.4 h) and diel periodicities (24 h), with the diel periodicity generally being stronger.

3.5.2. Case study of an extreme rain event

A total of 13 heavy rain events (24 h rainfall > 5 cm after Fagan et al., 2004) occurred during the study period, primarily in September–December 2016 and April–June 2017. The largest rain event occurred in late April 2017 with rainfall from 23 April 2017 02:48 to 28 April 2017 12:58, during which 13.9 cm of

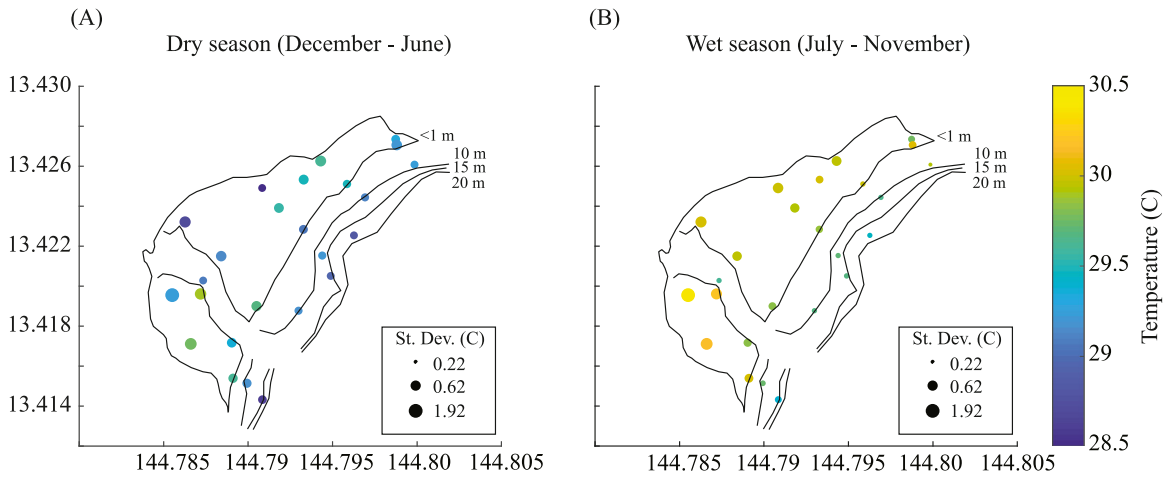

Fig. 7. Mean temperature in Pago Bay during the (A) dry and (B) wet seasons. Each measurement site is marked by a circle; the color of the circle indicates mean temperature. The size of the circle indicates the standard deviation. Lines indicating isobaths of the reef crest (<1 m) and on the fore reef (10 m, 15 m, and 20 m) are shown. (For interpretation of the references to color in this figure legend, the reader is referred to the web version of this article.)

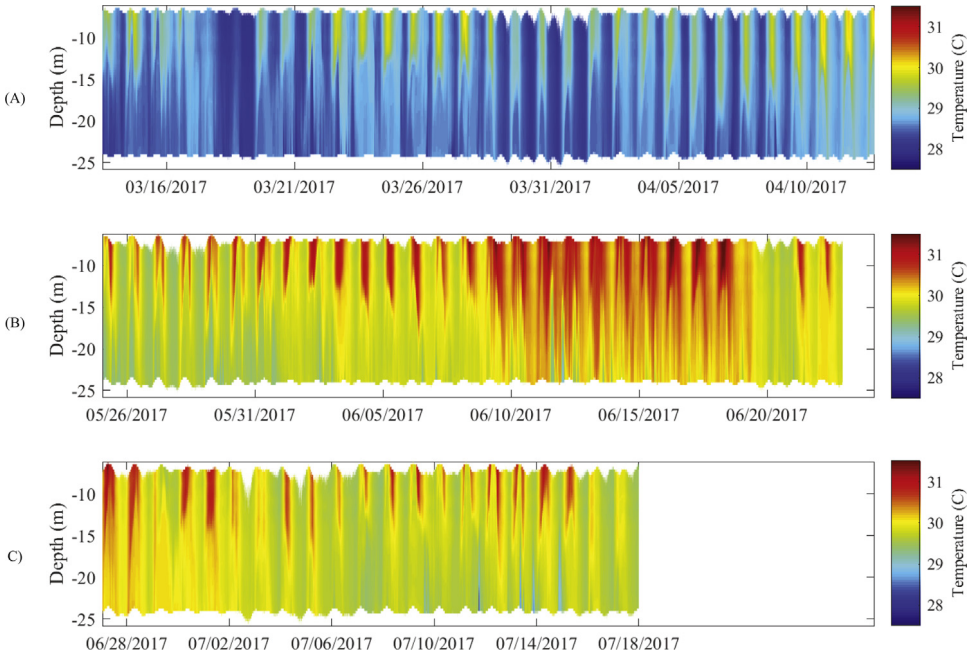

Fig. 8. Water column temperature (°C) in the Pago Bay channel for the 3 deployments where pressure records were available: (A) March to April 2017, (B) May to June 2017, and (C) June to July 2017. The deployment from August–October 2016 did not have pressure sensors for depth correction; data are shown in Fig. S10. Date format on the *x*-axis is MM/DD/YYYY.

rain fell in three days after 133 days without any significant rainfall (Fig. 11G). The effects of this rainfall were seen in several of the channel parameters. Salinity decreased by 1.27 PSS below the previous 14-day mean (Fig. 12B), and a 1.23 mg/m^3 increase in fluorescence was observed above the 14-day mean (Fig. 12C). The first large drop in salinity occurred 3 h earlier than the beginning of the fluorescence increase. An increase in turbidity was observed up to 24.14 NTU higher than the 14-day mean (Fig. 12F). The daily range in pH during the storm event dropped as low as 0.12, compared to the previous 14 days with ranges of 0.18 to 0.26 (Fig. 12D). Estimated backscatter observed by the current profiler on the mooring also showed an abrupt increase. The estimated backscatter during the acute rain-associated backscatter increase was 25.29 dB above background levels, which equates to an increase by a factor of 337. The overall geometric mean backscatter reading for the day of the spike was a factor of 7.5 times higher than background (Fig. 12H).

Other instances of sudden backscatter increases were identified throughout the study. There were eight instances where the daily geometric mean of backscatter was 7.5 to 25.7 times higher than the previous day, indicating that these increases were of comparable or greater severity than the examined case study. Five of these additional backscatter increases also occurred during heavy rain events. The remaining three increases occurred during rapid wave height increases of $>$ 1.6 m. The water quality sensors were not collecting data during these other events, but it is possible that similar changes in water quality as observed in the April 2017 rain event may have occurred, particularly during events associated with rain. A generalized additive model of estimated backscatter in the channel with rainfall and wave height as predictors explained 64.8% of the variability in backscatter. Both predictors were significant and had a positive relationship to estimated backscatter. Details of the GAM are shown in Table S4 and Fig. S11. (See Fig. 12.)

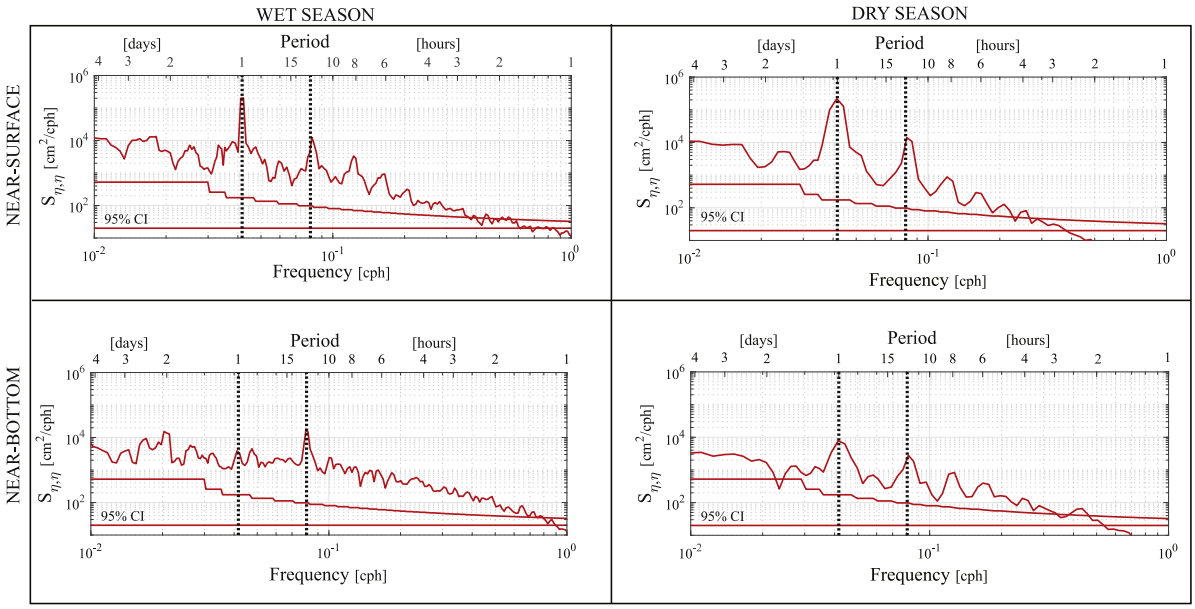

Fig. 9. Power spectral density (PSD) results from the temperature chain. PSD plots are shown for near-surface and near-bottom sensors. A sample spectrum is shown for each during a wet season deployment (August–October 2016, 1st column) and a dry season deployment (March–April 2017, 2nd column). Dashed lines show the 24 h and 12.4 h periods.

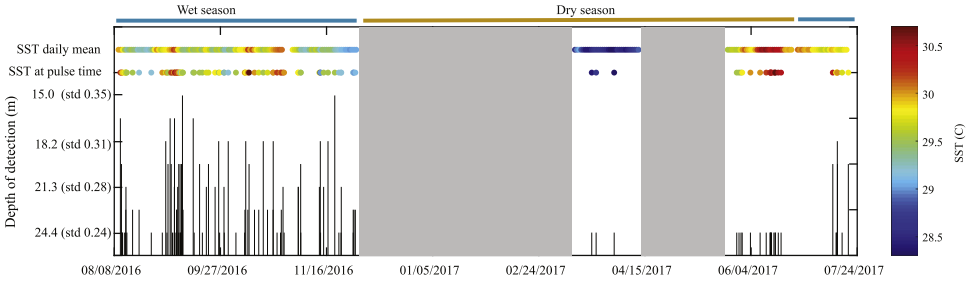

Fig. 10. Time of observed cold pulses versus depth of detection (black vertical lines) measured at the temperature chain in the channel of Pago Bay. The SST at the time of the observed cold pulse and the daily SST mean throughout the thermistor chain deployments is shown in color, with blue indicating cooler sea surface temperature and red indicating higher sea surface temperature. The wet season is indicated by the blue bar, and the dry season is indicated by the orange bar. Grey boxes indicate times when the thermistor chain was not collecting data. The standard deviation in depth reflects changes in sensor depth due to currents increasing the angle of the t-chain. Date format on the *x*-axis is MM/DD/YYYY. (For interpretation of the references to color in this figure legend, the reader is referred to the web version of this article.)

4. Discussion

4.1. Circulation in Pago Bay

Circulation in Pago Bay had characteristics of typical fringing reef circulation patterns. The reef flat and channel both had consistent unidirectional flow, and the reef flat and channel current magnitudes were strongly driven by wave height. With larger waves, more water is being moved onto the reef flat and therefore more water is moved back out to the open ocean via the channel, so current speeds increase. This pattern of circulation in fringing reefs has been observed in coastal systems all over the world (Coronado et al., 2007; Hench et al., 2008; Storlazzi et al., 2006; Taebi et al., 2011), including in other bays in Guam (Péquignet et al., 2011; Vetter et al., 2010). During days with very low tides, the mean daily velocity on the reef flat was lower. This observation is likely due to large areas of the reef flat that are dry and exposed during extreme lows, along with reduced water transport over the reef crest during low tides. Together, this disrupts normal flow patterns and results in more stagnant reef flat water.

Wind and wave direction have a small but significant impact on water speed on the reef flat. As the direction of waves and wind become closer to directly across-shore, current magnitude on the reef flat increases.

Flow on the fore reef was more affected by wind direction than flow on the reef flat and channel. Changes in wind direction corresponded to changes in both current speed and current direction. Reversals of current direction during trade wind conditions vs. non-trade wind conditions were observed on the southern fore reef, close to the channel mouth. The fate of water exiting the channel may therefore be different on trade wind days, when it is more likely to be transported south along the coast of Guam, as compared to non-trade wind days where the plume from the channel may carried to the north.

Previous work on the circulation in Pago Bay used dye-tracer methods on the reef flat (Marsh et al., 1982). The dye tracer study's results were supported by results from this study on the north reef flat via current profiler and on the south reef flat via temperature observations. In the south reef flat, Marsh et al. (1982) identified a circulation cell of restricted water flushing. The south reef flat current profiler in this study was deployed in that cell, and the observed mean flow was towards shore and the channel. However, that water could get entrained in the circulation cell and remain in the area longer. Temperature observations from this study within the circulation cell had the

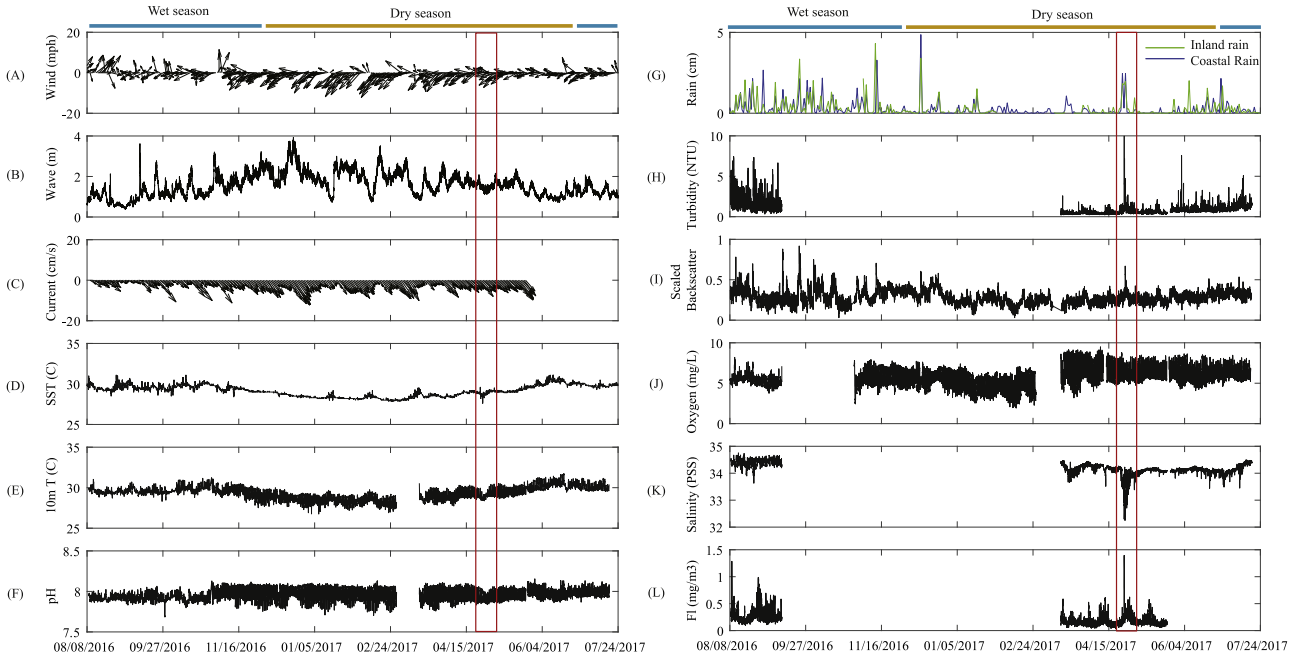

Fig. 11. Time series plots of (A) wind (mph), (B) wave height (m), (C) daily subtidal currents (cm/s), (D) sea surface temperature (SST) (°C), (E) temperature at 10 m depth (T) (°C), (F) pH, (G) rain (cm), (H) turbidity (NTU), (I) backscatter, normalized on a scale of 0 to 1, (J) dissolved oxygen (mg/L), (K) salinity (PSS), and (L) fluorescence (mg/m^3). Variables are shown from 8 August 2016 to 24 July 2017. Plots C, E, F, and H-L show oceanographic measurements collected in the Pago Bay channel for this study; plots A, B, D, and G are additional environmental data. The red rectangles highlight an extreme rainfall event (see Section 3.5.2). Date format on the *x*-axis is MM/DD/YYYY.

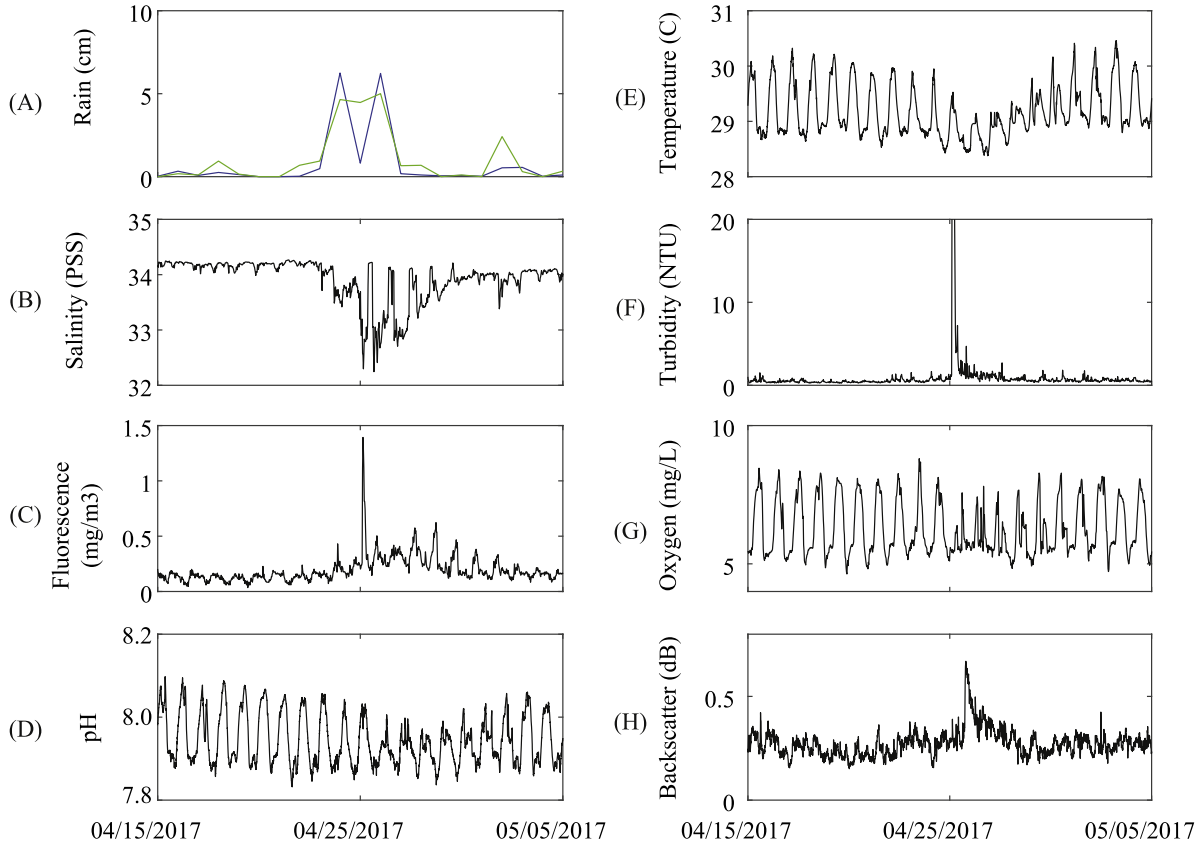

Fig. 12. Time series observations from the Pago Bay channel at 10 m from 15 April 2017–5 May 2017, highlighting the storm event on 23–28 April 2017. Time series plots are shown for (A) rain, (B) salinity, (C) fluorescence, (D) pH, (E) Temperature, (F) turbidity, (G) oxygen, and (H) scaled estimated backscatter. Date format on the *x*-axis is MM/DD/YYYY.

highest magnitude and highest daily heating, which supports that water was retained in this area longer and subject to more solar heating. This study expanded on the Marsh et al. (1982) study by monitoring a much longer time series, by observing current flow in the channel and fore reef, and by discerning the effects of wind, waves, and tides on flow patterns.

4.2. Temporal–spatial variability in temperature and oxygen

Temperatures in Pago Bay were warmer in the wet season and the mean temperature patterns were fairly consistent throughout the bay, but the reef flat had extreme diel temperature fluctuations that occasionally were over 9 °C. The highest temperature and daily temperature ranges were observed in the southern, inshore reef flat where circulation patterns result in longer water residence times (Marsh et al., 1982) and river water may intrude.

Corals living in different areas of the reef can acclimate to different levels of thermal variability, and factors other than temperature contribute to whether corals can survive in a particular habitat, especially solar irradiance (Fitt et al., 2001). In exceptional circumstances, some corals have been observed to withstand regular temperature fluctuations of 6 °C (Oliver and Palumbi, 2011). However, temperature fluctuations of the magnitude measured on the reef flat may be well over the limit of coral thermal tolerance. In addition to occasional extreme temperature fluctuations, the reef flat also has high solar radiation exposure due to its shallow depth, and areas close to the channel experience sudden increases in turbidity during rain events that could inhibit photosynthesis for several days. All of these factors may contribute to the lack of a coral community on the Pago Bay reef flat. Corals are much more abundant on the fore reef, where mean temperatures are very similar to the reef flat but diel variability due to solar insolation is lower. Future research will measure temperature and solar irradiance in fore reef habitats in Guam to better characterize the environmental limits associated with bleaching events in this community.

The turf and macroalgal community that is prevalent on the reef flat appeared to drive daily variation in dissolved oxygen via photosynthesis. While flow can enhance photosynthesis by driving the efflux of oxygen from algae, seagrass, and coral tissues (Finelli et al., 2006; Mass et al., 2010), and wind can increase dissolved oxygen at the air–sea interface, the variability in dissolved oxygen we observed was not correlated to currents or wind and dissolved oxygen concentrations increased during the day, pointing to photosynthesis as the primary driver of oxygen variability in Pago Bay. The observed higher dissolved oxygen measurements with higher temperatures on the reef flat may be due to a high temperature optimum for photosynthesis in the benthic algae (Kirk, 1983).

4.3. Cold pulses

Cold pulses were observed in the deeper part of the water column near the mouth of the Pago Channel, and these pulses occurred more frequently when sea surface temperatures were higher. The cold pulses were likely driven by internal waves on a tidal frequency since strong tidal fluctuations were observed at the deeper part of the water column during the time periods when most pulses were observed. Previous modeling work has suggested that large internal waves may propagate around Guam (Wolanski et al., 2003), and these cold pulse observations also suggest that these internal waves exist.

A strongly stratified water column may allow more intrusion of deep water to shallower depths than a well-mixed water column (Leichter et al., 1996), and water column stratification may vary seasonally with wind and temperature. The most extreme cold pulses observed in Pago Bay resulted in a 1.3 °C decrease in temperature within 5 min. On Florida's Conch Reef, cold pulses produced temperature decreases of up to 5.4 °C (Leichter et al., 1996), and in Hawaii, maximum observed cold pulses ranged from 1.08–1.52 °C (Sevadjian et al., 2012).

The pulses were observed at 15–26 m depth, and at this depth the benthic cover in Pago Bay is a mix of coral and turf algae, with turf algae increasing with depth. Cold pulses can play an important role in reef nutrient cycling and ecology by bringing nutrient-rich cooler water to shallower depths (Leichter et al., 2003; Sevadjian et al., 2012) and by transporting phytoplankton assemblages along slopes (Sevadjian et al., 2012). Where the cold pulses intersect with coral reef habitat, they can provide a thermal refuge for corals in the face of rising ocean temperatures. Internal waves have been shown to reduce coral mortality from bleaching events even during periods of anomalously high sea surface temperatures (Wall et al., 2015), and in addition to relief from temperature stress corals may additionally benefit from increased salinity and biotic and abiotic material available in the pulse water (Storlazzi et al., 2013).

4.4. Oceanographic response to an extreme storm event

Rain events and the associated runoff and sedimentation are major threats to Guam's marine benthic habitats (Gawel, 1999; Prouty et al., 2014; Richmond, 1993; Wolanski et al., 2003) (Fig. 13). The high sedimentation rates in Guam are related to land-use practices that remove vegetation, such as intentionally-set wildfires, agriculture, and construction (Burdick et al., 2008; Minton, 2006). Sedimentation has significant biological and physical impacts on reef ecosystems by increasing turbidity, reducing light availability to organisms, smothering benthic organisms, reducing coral recruitment, acting as a vector for pollution such as persistent organic pollutants, sewage, and heavy metals to reef environments, and decreasing reef productivity, calcification, and accretion (Burdick et al., 2008; Rogers, 1990).

The large storm event examined in this study resulted in elevation of turbidity, fluorescence, and estimated backscatter, and a depression in salinity and in the variability of dissolved oxygen, temperature, and pH that persisted for one week. Smaller rain events likely cause similar changes in surface waters that were not detected by our 10 m sensors. While the sinking rate of the sediment is not known, it is apparent from field observations that sediment settles in the channel, on the reef flat adjacent to the channel, and on the fore reef. Sediment that does get flushed out of the channel could become entrained in the observed alongshore flow on the fore reef and eventually sink onto the fore reef coral habitat, with the direction of flow being dependent on wind conditions. During high wave conditions (which lead to faster flow out the channel) more sediment may be exported to the fore reef area and become entrained in alongshore flow before sinking; during small wave conditions, flow magnitudes on the fore reef are very small, and the flow out the channel could export the sediment far offshore. Future research on sediment sinking rates and sediment accumulation in different areas in and surrounding the channel would allow a better understanding of the fate of the sediment and the scale of the impact to fore reef coral ecosystems.

Rain events of the magnitude examined in this study are not uncommon. Eight other events caused increases in backscatter in the channel of similar or greater magnitude during the study period. Five of these backscatter increases occurred during other large-scale rain events, and three occurred during rapid increases in wave height, which indicates that while rain is usually the trigger for increase in turbidity and backscatter, waves can cause sediment resuspension. If the sedimentation impact on

Fig. 13. Photo of Pago Bay, Guam following heavy sediment input related to coastal development. Image credit: Jason S. Biggs, University of Guam Marine Laboratory.

coral habitat in this region is found to be significant in further study, land-based erosion mitigation strategies may be called for.

Recent work on erosion mitigation on the island of Lanai, Hawaii, USA demonstrated that community-constructed gabion dams using local invasive plant species significantly reduced the amount of sediment exported to the reef over the course of one year (Teneva et al., 2016). A similar installation of semi-permeable dams in rivers in damaged watersheds of Guam could slow water flow during rain events enough to reduce the amount of sediment that reaches the coral reef systems, while still allowing freshwater organisms to move through their native habitat.

4.5. Conclusions

This study provides a baseline of the physical oceanographic patterns and processes of Pago Bay, Guam. In addition, this study provides insights into the daily to seasonal fluctuations in the temperature and dissolved oxygen environment, as well as to the scales of variability of nutrients and pH. This study also provides detailed observations of the impacts of a rain event on water quality in Pago Bay.

Observations of circulation expanded on the existing Marsh et al. (1982) model of circulation in Pago Bay. On timescales of days to seasons, wave height, wind and wave direction, and to a small extent neap/spring tide cycles had an influence on the observed water speed. Higher wave heights and wave and wind directions that were across-shore drove faster current speeds throughout the bay.

Temperature and dissolved oxygen were also mapped throughout the bay for a period of a year. These maps show that diel variation was dominant over tidal variation, and that diel variation was stronger in shallower areas, and strongest in the southern reef flat. Observations of temperature in the water column revealed that internal waves can propagate cooler, deeper water up to 15 m depth, and these intermittent cold pulses should not be overlooked when considering the overall thermal habitat of organisms living on the deeper fore reef. The spatial and temporal observations of circulation, temperature, and dissolved oxygen in Pago Bay provided an essential baseline understanding of the physical system for future ecological studies and assessments of changes in the watershed.

Finally, the scales of variability of oceanographic and water quality parameters in the channel were documented. The impact of a large rain event on the normal cycles was observed. Destabilization of sediment in the Pago River watershed leads to heavy sediment influx to Pago Bay during rain events, and based on our circulation and estimated backscatter results, the southern fore reef may be at a higher risk than the northern fore reef for sedimentation deposition associated with flow out the Pago Channel during normal trade wind conditions. Future work will move towards a better understanding of reef resilience in Guam by examining coral susceptibility to bleaching within the context of the observed flow regime, temperature environment, and storm impacts using genetic tools in combination with observations.

Acknowledgments

We would like to acknowledge and thank Marine Technicians Joe Cummings and Jason Miller; Dive Safety Officers John Peralta and Dave Pence; University of Guam professor Mark Lander for rain data; and University of Guam EPSCoR students: Matt Mills, Devin Resko, Alisha Gill, James Fifer, Diona Drake, and Andrew Kang for assistance in the field. We would also like to thank Anna Neuheimer, Johanna Wren, and Kyle Edwards for discussions regarding statistical modeling, Jim Potemra for assistance with GIS mapping, and Assaf Azouri for input on spectral analysis.

Funding

This work was supported by the National Science Foundation, USA under Grant Number OIA-1457769 and the National Oceanic and Atmospheric Administration (NOAA), USA through PacIOOS award NA16NOS0120024.

Appendix A. Supplementary data

Supplementary material related to this article can be found online at https://doi.org/10.1016/j.rsma.2019.100740.

References

Anthony, K.R.N., Ridd, P.V., Orpin, A.R., Larcombe, P., Lough, J., 2004. Temporal variation of light availability in coastal benthic habitats: Effects of clouds, turbidity, and tides. Limnol. Oceanogr. 49 (6), 2201–2211.

Barton, K., 2009. MuMIn: Multi-Model Inference. R package version 0.12. 0. http://r-forger-project.org/projects/mumin/.

Becker, J.M., Merrifield, M.A., Ford, M., 2014. Water level effects on breaking wave setup for Pacific island fringing reefs. J. Geophys. Res. Ocean. 119 (2), 914–932.

Burdick, D., Brown, V., Asher, J., Caballes, C., Gawel, M., Goldman, L., Hall, A., Kenyon, J., Leberer, T., Lundblad, E., 2008. Status of the Coral Reef Ecosystems of Guam. Bureau of Statistics and Plans, Guam Coastal Management Program, iv.

Clark, S.J., 2013. The Influence of a Cross-Reef Channel on Circulation over a Fringing Reef At Ipan, Guam (Master's thesis). University of Hawaii at Manoa, Honolulu.

Coronado, C., Candela, J., Iglesias-Prieto, R., Sheinbaum, J., López, M., Ocampo-Torres, F., 2007. On the circulation in the Puerto Morelos fringing reef lagoon. Coral Reefs 26, 149–163.

Craig, P., Birkeland, C., Belliveau, S., 2001. High temperatures tolerated by a diverse assemblage of shallow-water corals in American Samoa. Coral Reefs 20, 185–189.

Deines, K.L., 1999. Backscatter estimation using broadband acoustic Doppler current profilers. In: Proceedings of the IEEE Sixth Working Conference on Current Measurement. IEEE, pp. 249–253.

Fabricius, K.E., 2005. Effects of terrestrial runoff on the ecology of corals and coral reefs: review and synthesis. Mar. Pollut. Bull. 50, 125–146.

Fagan, K., MacKenzie, F., Andersson, A., 2004. Processes Controlling Air-Sea Exchange of CO2 in a Subtropical Pacific Estuary, AGU Fall Meeting Abstracts.

Finelli, C.M., Helmuth, B.S., Pentcheff, N.D., Wethey, D.S., 2006. Water flow influences oxygen transport and photosynthetic efficiency in corals. Coral Reefs 25, 47–57.

Fitt, W.K., Brown, B.E., Warner, M.E., Dunne, R.P., 2001. Coral bleaching: interpretation of thermal tolerance limits and thermal thresholds in tropical corals. Coral reefs 20 (1), 51–65.

Fox, J., Weisberg, S., Adler, D., Bates, D., Baud-Bovy, G., Ellison, S., Firth, D., Friendly, M., Gorjanc, G., Graves, S., 2012. Package 'Car' Vienna: R Foundation for Statistical Computing.

Fulton, C., Bellwood, D., Wainwright, P., 2005. Wave energy and swimming performance shape coral reef fish assemblages. Proc. R. Soc. Lond. Ser. B: Biol. Sci. 272, 827–832.
Gawel, M.J., 1999. Protection of marine benthic habitats in the Pacific Islands. A case study of Guam. Oceanol. Acta 22, 721–726.
Hatcher, B.G., 1990. Coral reef primary productivity. A hierarchy of pattern and process. Trends Ecol. Evol. 5, 149–155.
Hench, J.L., Leichter, J.J., Monismith, S.G., 2008. Episodic circulation and exchange in a wave-driven coral reef and lagoon system. Limnol. Oceanogr. 53, 2681–2694.
Kirk, J.T.O., 1983. Light & Photosynthesis in Aquatic Ecosystems, second ed. Cambridge, Great Britain, pp. 333–338.
Leichter, J.J., Stewart, H.L., Miller, S.L., 2003. Episodic nutrient transport to Florida coral reefs. Limnol. Oceanogr. 48, 1394–1407.
Leichter, J.J., Wing, S.R., Miller, S.L., Denny, M.W., 1996. Pulsed delivery of subthermocline water to Conch Reef (Florida Keys) by internal tidal bores. Limnol. Oceanogr. 41, 1490–1501.
Lowe, R.J., Falter, J.L., Monismith, S.G., Atkinson, M.J., 2009. Wave-driven circulation of a coastal reef–lagoon system. J. Phys. Oceanogr. 39, 873–893.
Marsh, J., Ross, R.M., Zolan, W.J., 1982. Water circulation on two Guam reef flats. In: Proceedings of the 4th International Coral Reef Symposium. Marine Sciences Center, University of Philippines, Manila, Philippines, pp. 355–360.
Mass, T., Genin, A., Shavit, U., Grinstein, M., Tchernov, D., 2010. Flow enhances photosynthesis in marine benthic autotrophs by increasing the efflux of oxygen from the organism to the water. Proc. Natl. Acad. Sci. 107, 2527–2531.
MATLAB Release, 2017. The MathWorks. Inc. Natick, Massachusetts, United States.
Mazerolle, M.J., Mazerolle, M.M.J., 2017. Package 'AICcmodavg' R Package.
McClanahan, T., Maina, J., 2003. Response of coral assemblages to the interaction between natural temperature variation and rare warm-water events. Ecosystems 6, 551–563.
McManus, M.A., Benoit-Bird, K.J., Woodson, C.B., 2008. Behavior exceeds physical forcing in the diel horizontal migration of the midwater sound-scattering layer in Hawaiian waters. In: MEPS, vol. 365, http://dx.doi.org/10.3354/meps07491, 91–101.
Minton, D., 2006. Fire, Erosion, and Sedimentation in the Asan-Piti Watershed and War in the Pacific NHP, Guam.
Monismith, S.G., Genin, A., Reidenbach, M.A., Yahel, G., Koseff, J.R., 2006. Thermally driven exchanges between a coral reef and the adjoining ocean. J. Phys. Oceanogr. 36, 1332–1347.
Nortek, 2017. The Comprehensive Manual. Nortek Headquarters, Rud, Norway.
Nyström, M., Folke, C., Moberg, F., 2000. Coral reef disturbance and resilience in a human-dominated environment. Trends Ecol. Evol. 15, 413–417.
Oliver, T., Palumbi, S., 2011. Do fluctuating temperature environments elevate coral thermal tolerance? Coral Reefs 30, 429–440.
Onset, 2012. HOBO Dissolved Oxygen Logger (U26-001) Manual. Onset Computer Corporation, Bourne, MA.
Ostrander, C.E., McManus, M.A., DeCarlo, E.H., Mackenzie, F.T., 2008. Temporal and spatial variability of freshwater plumes in a semienclosed estuarine–bay system. Estuaries Coasts 31 (192).
Pastorok, R.A., Bilyard, G.R., 1985. Effects of sewage pollution on coral-reef communities. In: Marine Ecology Progress Series, vol. 21, Oldendorf, pp. 175–189.
Péquignet, A.-C., Becker, J., Merrifield, M., Boc, S., 2011. The dissipation of wind wave energy across a fringing reef at Ipan, Guam. Coral Reefs 30, 71–82.
Piniak, G.A., Storlazzi, C.D., 2008. Diurnal variability in turbidity and coral fluorescence on a fringing reef flat: Southern Molokai, Hawaii. Estuar. Coast. Shelf Sci. 77, 56–64.
Prouty, N.G., Storlazzi, C.D., McCutcheon, A.L., Jenson, J.W., 2014. Historic impact of watershed change and sedimentation to reefs along west-central Guam. Coral Reefs 33 (733).
Putnam, H.M., Edmunds, P.J., 2011. The physiological response of reef corals to diel fluctuations in seawater temperature. J. Exp. Mar. Biol. Ecol. 396, 216–223.
R Core Team, (2017). R: A language and environment for statistical computing. R Foundation for Statistical Computing, Vienna, Austria. URL https://www.R-project.org/.
Richmond, R.H., 1993. Coral reefs: present problems and future concerns resulting from anthropogenic disturbance. Amer. Zool. 33, 524–536.
Rogers, C.S., 1990. Responses of coral reefs and reef organisms to sedimentation. In: Marine Ecology Progress Series, vol. 62, Oldendorf, pp. 185–202.
Ryan, J.P., McManus, M.A., Chavez, F.P., 2008. Phytoplankton thin layers caused by shear in frontal zones of a coastal upwelling system. Mar. Ecol. Prog. Ser. 354, 21–34.
Sarkar, D., 2008. Lattice: Multivariate Data Visualization with R. Springer Science & Business Media.
Satlantic, Inc., 2016. Submersible Ultraviolet Nitrate Analyzer (SUNA) User Manual. Sea-Bird Coastal, Bellevue, WA.
Sevadjian, J., McManus, M., Benoit-Bird, K., Selph, K., 2012. Shoreward advection of phytoplankton and vertical re-distribution of zooplankton by episodic near-bottom water pulses on an insular shelf: Oahu, Hawaii. Cont. Shelf Res. 50, 1–15.
SonTek/YSI, 2000. ADP Acoustic Doppler Profiler Technical Documentation. SonTek/YSI, San Diego, CA.
Storlazzi, C.D., Field, M.E., Cheriton, O.M., Presto, M.K., Logan, J.B., 2013. Rapid fluctuations in flow and water-column properties in Asan Bay, Guam: implications for selective resilience of coral reefs in warming seas. Coral Reefs 32 (4), 949–961.
Storlazzi, C., McManus, M., Logan, J., McLaughlin, B., 2006. Cross-shore velocity shear, eddies and heterogeneity in water column properties over fringing coral reefs: West Maui, Hawaii. Cont. Shelf Res. 26, 401–421.
Storlazzi, C.D., Ogston, A.S., Bothner, M.H., Field, M.E., Presto, M., 2004. Wave-and tidally-driven flow and sediment flux across a fringing coral reef: Southern Molokai, Hawaii. Cont. Shelf Res. 24, 1397–1419.
Taebi, S., Lowe, R.J., Pattiaratchi, C.B., Ivey, G.N., Symonds, G., Brinkman, R., 2011. Nearshore circulation in a tropical fringing reef system. J. Geophys. Res. Ocean. 116.
Teneva, L., McManus, M., Jerolmon, C., Neuheimer, A., Clark, S., Walker, G., Kaho'ohalahala, K., Shimabukuro, E., Ostrander, C., Kittinger, J., 2016. Understanding reef flat sediment regimes and hydrodynamics can inform erosion mitigation on land. Collabra: Psychology 2.
Vetter, O., Becker, J.M., Merrifield, M.A., Pequignet, A.C., Aucan, J., Boc, S.J., Pollock, C.E., 2010. Wave setup over a Pacific Island fringing reef. J. Geophys. Res. Ocean. 115.
Wall, M., Putchim, L., Schmidt, G.M., Jantzen, C., Khokiattiwong, S., Richter, C., 2015. Large-amplitude internal waves benefit corals during thermal stress. Proc. R. Soc. Lond. [Biol.] 282 (1799), 20140650.
Wolanski, E., Richmond, R.H., Davis, G., Bonito, V., 2003. Water and fine sediment dynamics in transient river plumes in a small, reef-fringed bay, guam. Estuar. Coast. Shelf Sci. 56, 1029–1040.
Wood, S.N., 2001. mgcv: GAMs and generalized ridge regression for R. R News 1, 20–25.
Zuur, A.F., 2012. A Beginner'S Guide to Generalized Additive Models with R. Highland Statistics Limited Newburgh, NY, USA.
Zuur, A.F., Ieno, E.N., Elphick, C.S., 2010. A protocol for data exploration to avoid common statistical problems. Methods Ecol. Evol. 1, 3–14.